Dyes and Pigments 91 (2011) 413–421

Contents lists available at ScienceDirect

Dyes and Pigments

journal homepage: www.elsevier.com/locate/dyepig

Novel yellow phosphorescent iridium complexes containing a carbazole–oxadiazole unit used in polymeric light-emitting diodes

Huaijun Tang, Yanhu Li, Caihong Wei, Bing Chen, Wei Yang*, Hongbin Wu, Yong Cao

Institute of Polymer Optoelectronic Materials and Devices, Key Lab of Specially Functional Materials of the Ministry of Education, South China University of Technology, Guangzhou 510640, PR China

ARTICLE INFO

Article history:
Received 2 November 2010
Received in revised form
30 March 2011
Accepted 3 April 2011
Available online 21 April 2011

Keywords:
Iridium complex
Carbazole
Oxadiazole
Polymeric light-emitting diode
Electroluminescence
White-light

ABSTRACT

Yellow iridium complexes $Ir(PPOHC)_3$ and $(PPOHC)_2Ir(acac)$ (PPOHC: 3-(5-(4-(pyridin-2-yl)phenyl)-1,3,4-oxadiazol-2-yl)-9-hexyl-9*H*-carbazole) were synthesized and characterized. The $Ir(PPOHC)_3$ complex has good thermal stability with 5% weight-reduction occurring at 370 °C and a glass-transition temperature of 201 °C. A polymeric light-emitting diode using the $Ir(PPOHC)_3$ complex as a phosphorescent dopant showed a luminance efficiency of 16.4 cd/A and the maximum external quantum efficiency of 6.6% with CIE coordinates of (0.50, 0.49). A white polymeric light-emitting diode was fabricated using $Ir(PPOHC)_3$ which showed a luminance efficiency of 15.3 cd/A, with CIE coordinates of (0.39, 0.44). These results indicate that the iridium complexes containing a linked carbazole–oxadiazole unit are promising candidates in high-efficiency electroluminescent devices.

1. Introduction

Organic light-emitting diodes (OLEDs) are under intense investigation because of their potential applications in full-colour flat-panel displays, back-lit liquid crystal displays and solid-state lighting sources [1–6]. Among electroluminescent (EL) materials, the heavy transition metals, e.g. Pt(II) and Ir(III), complex phosphors have attracted more attention, because both singlet and triplet excitons can be harvested to generate light, in principle, their theoretical internal quantum efficiency (QE) can be as high as 100%, rather than the inherent 25% upper limit only from the radiative decay of singlet excitons of the fluorescent precursors [7–10]. EL materials also can be classified into small-molecule and polymer materials according to the molecular weight, thus there are two device fabrication technologies, vacuum-deposition (mostly based on small-molecule materials) and solution processing (mostly based on polymer materials). Compared with vacuum-deposition, solution processing technology can offer some unique advantages, such as low-cost, easy-processibility over a large surface area by spin-coating, ink-jet printing, or screen-printing, and better control of the level of the dopants [11–13]. In the past few years, small-molecule complex phosphors doped polymeric light-emitting diodes (PLEDs) have been developed rapidly, because such devices have brought together the advantages of solution-processed technology and the high-efficiency of small-molecule materials [13–19]. For use in such EL devices, the small-molecule phosphors are required to possess high solubility, high morphological and thermal stabilities as well as high EL efficiency. Delightfully, the properties such as emitting color, solubility, morphological and thermal stabilities, even the efficiency of the metal complex phosphors can be intentionally obtained via reasonable molecular design by employing appropriate functional groups on the ligands [7,20].

Groups such as carbazole, triphenylamine and oxadiazole with hole or electron-transporting functions are beneficial to improving the performance of EL materials [7,20–29]. Recently, the synergic action of hole and electron-transporting functional groups has attracted great attention, because it can provide balance in electron and hole fluxes and thus simplifies the device structure [24]. For example, a series of bipolar triphenylamine/oxadiazole or carbazole/oxadiazole derivatives have been synthesized and used as highly efficient host materials [24–26]. Novel Pt(II) complexes containing hole-transporting triarylamine and electron-transporting oxadiazole have been synthesized and used as phosphor guests [27]. Triarylamine and oxadiazole substituted ferrocenes have been used as hole-injection materials in polymeric light-emitting diodes [28]. A Eu(III) complex containing carbazole and oxadiazole has been synthesized and used as a red light emitter [29].

* Corresponding author. Fax: +86 20 87110606.
E-mail address: pswyang@scut.edu.cn (W. Yang).

0143-7208/$ – see front matter © 2011 Elsevier Ltd. All rights reserved.
doi:10.1016/j.dyepig.2011.04.005

Besides three primary colors of red, green and blue (RGB), yellow not only is another important monochromatic light, but also is a key component in generating efficient white-light. For example, a yellow iridium complex bis(2-(9,9-diethyl-9*H*-fluoren-2-yl)-1-phenyl-1*H*-benzoimidazol-N,C^3) iridium(acetylacetonate) ($(fbi)_2Ir(acac)$) was synthesized and used for fabricating highly efficient white OLEDs with blue iridium complex bis(2-(4,6-difluorophenyl)-pyridinato-N,C^2) picolinate iridium(III) (FIrpic) [30–32]. Several yellow or orange–yellow iridium complexes using 2-(9,9-diethylfluoren-2-yl)pyridine (Flpy) or its derivatives as ligands were synthesized and also used for fabricating highly efficient white OLEDs with FIrpic [13,14,33,34]. A yellow iridium complex iridium(III) bis[3-phenylisoquinoline](2-(2*H*-1,2,4-triazol-3-yl)pyridine) ($Ir(3\text{-}piq)_2(pt)$) was used for fabricating white PLEDs with the blue emission of host materials polyfluorene (PFO) [35]. In this work, the ligand 3-(5-(4-(pyridin-2-yl)phenyl)-1,3,4-oxadiazol-2-yl)-9-hexyl-9*H*-carbazole (PPOHC) containing a carbazole–oxadiazole unit and the derived yellow homoleptic complex $Ir(PPOHC)_3$ and heteroleptic complex $(PPOHC)_2Ir(acac)$ (acac:acetylacetone) were synthesized and used in yellow and white polymeric light-emitting diodes.

2. Experimental

2.1. Synthesis and characterization of the iridium(III) complexes

2.1.1. General information

Chemicals and reagents were obtained from commercial sources, and used without further purification unless otherwise noted. Column chromatography was carried out on silica gel (200–300mesh). Yields refer to the isolated pure compound. ^{1}H NMR spectra were recorded on a Bruker AV300 spectrometer operating at 300 MHz, tetramethylsilane (TMS) was used as internal standard. IR spectra were recorded with a Bruker Vector 33 spectrometer. Elemental analyses were performed on Vario EL Elemental Analysis Instrument (Elementar Co.). Ultraviolet–visible (UV–Vis) absorption spectra were recorded on a HP8453E spectrophotometer (Hewlett–Packard Co.). Photoluminescence (PL) spectra were recorded on an Fluorolog–3 spectrophotometer (Jobin Yvon Inc.). Differential scanning calorimetry (DSC) curves were measured on a Netzsch DSC200 analyzer at a heating rate 10 °C/min under N_2. In DSC measurements of the iridium complexes, both of them underwent two heating cycles, the second heating followed the first heating–cooling cycle (the first heating was from room temperature to 250 °C). Thermogravimetry (TG) curves were measured on a Netzsch TG209 thermal analyzer at a heating rate 10 °C/min under N_2. Mass spectra were obtained from a Bruker Esquire HCT PLUS liquid chromatography/mass spectrometer(LC/MS, Bruker Corp.) with an electrospray ionization (ESI) interface using acetonitrile as the matrix solvent. Cyclic voltammetry (CV) was measured on a computer-controlled CHI800C electrochemical analyzer (Shanghai Chenhua Instrument Co.). Anhydrous and Ar–saturated dichloromethane solutions of the iridium(III) complexes containing 0.1 mol/L tetra-n-butylammonium hexafluorophosphate ($TBAPF_6$) as the supporting electrolyte were scanned at 50 mV/s. A glass carbon electrode was used as a working electrode, a Ag/AgCl electrode was used as a reference electrode, a platinum wire was used as a counter electrode. Ferrocene (4.8 eV under vacuum) was used as the internal standard material.

2.1.2. 9-Hexyl-9H-carbazole **(1)**

After a mixture of KOH (14.00 g, 250.0 mmol) and carbazole (6.60 g, 40.0 mmol) in acetone (80 mL) was stirred for 30 min, another mixture of 1-bromohexane (9.9 g, 60.0 mmol) in acetone (20 mL) was added dropwise in with stirring, and the stirring was kept for 10 h after the addition was over. The reaction mixture was slowly poured into water (about 500 mL) with stirring. The mixture was extracted with CH_2Cl_2 (3 × 80 mL), washed with water and dried (anhydrous Na_2SO_4). The solvent was distilled off and the residue was chromatographed over silica gel, eluting with petroleum ether (60–90 °C)/$CH_3COOC_2H_5$ (volume ratio, 10:1). Yield 86% (8.53 g), colorless needles, mp 65 °C (DSC, lit. [36] mp 65.4–65.7 °C). ^{1}H NMR (300 MHz, $CDCl_3$, 25 °C, ppm): δ = 8.13 (*d*, 2H, ^3J = 7.8 Hz, ArH), 7.41–7.51 (*m*, 4H, ArH), 7.22–7.27 (*m*, 2H, ArH), 4.31 (*t*, 2H, ^3J = 7.2 Hz, −N−CH_2−), 1.84–1.93 (*m*, 2H, −N−C−CH_2−), 1.29–1.56 (*m*, 6H, −$(CH_2)_3$−), 0.90 (*t*, 3H, −CH_3). IR (KBr, cm^{-1}), 3050, 2954, 2923, 2855, 1897, 1777, 1593, 1484, 1452, 1325, 1238, 1216, 1151, 997, 749, 724. Element Anal. Calc. for $C_{18}H_{21}N$ (%): C, 86.01; H, 8.42; N, 5.57. Found (%): C, 85.86; H, 8.63; N, 5.51.

2.1.3. 3-Formyl-9-hexyl-9H-carbazole **(2)**

$POCl_3$ (2 mL, 21.5 mmol) was added dropwise into dried N,N-dimethylformamide (DMF, 25 mL) with stirring in an ice bath. Then 9-hexyl-9*H*-carbazole (5.02 g, 20.0 mmol) was added in, the mixture was solwly heated to and maintained at 80 °C for 6 h. The cooled reaction mixture was slowly poured into ice-water (about 200 mL), and neutralized with Na_2CO_3. The mixture was extracted with CH_2Cl_2 (3 × 50 mL), washed with water and dried (anhydrous Na_2SO_4). The solvent was distilled off and the residue was chromatographed over silica gel, eluting with petroleum ether (60–90 °C) and CH_2Cl_2 (volume ratio, 2:1). Yield 78% (4.35 g), brownish-yellow oil. ^{1}H NMR (300 MHz, $CDCl_3$, 25 °C, ppm): δ = 10.07 (*s*, 1H, −CHO), 8.55 (*d*, 1H, −ArH), 8.12 (*d*, 1H, ^3J = 7.8 Hz, −ArH), 7.98 (dd, 1H, ^3J = 8.4 Hz, −ArH), 7.50–7.55 (*m*, 1H, ArH), 7.34–7.44 (*m*, 2H, ArH), 7.29–7.31 (*t*, 1H, ArH), 4.25 (*t*, 2H, ^3J = 7.2 Hz, −N−CH_2−), 1.80–1.90 (*m*, 2H, −N−C−CH_2−), 1.25–1.39 (*m*, 6H, −$(CH_2)_3$−), 0.87 (*t*, 3H, −CH_3). IR (KBr, cm^{-1}), 3052, 2955, 2929, 2857, 2727, 1893, 1686, 1593, 1469, 1383, 1352, 1339, 1329, 1240, 1177, 1135, 807, 765, 748, 730. Element Anal. Calc. for $C_{19}H_{21}NO$ (%):C, 81.68; H, 7.58; N, 5.01. Found (%): C, 81.83; H, 7.69; N, 5.14.

2.1.4. 3-Cyano-9-hexyl-9H-carbazole **(3)**

Ammonia (25–28%, 50 mL) was added in the mixture of 3-formyl-9-hexyl-9*H*-carbazole (5.58 g, 20.0 mmol) in tetrahydrofuran (THF, 25 mL), then I_2 (5.58 g, 22.0 mmol) was added in and was stirred for 1.5 h. $Na_2S_2O_3$ was added in until the blackish–brown vanished. The reaction mixture was extracted with CH_2Cl_2 (3 × 30 mL), washed with water and dried (anhydrous Na_2SO_4). The solvent was distilled off and the residue was chromatographed over silica gel, eluting with petroleum ether (60–90 °C) and CH_2Cl_2 (volume ratio, 3:1). Yield 92% (5.14 g), white solid, mp 80 °C (DSC). ^{1}H NMR (300 MHz, $CDCl_3$, 25 °C, ppm): δ = 8.41 (*t*, 1H, ArH), 8.13 (dt, 1H, ^3J = 7.8 Hz, ArH), 7.72 (dd, 1H, ^3J = 8.4 Hz, ArH), δ = 7.55–7.57 (*m*, 1H, ArH), 7.44–7.49 (*m*, 2H, ArH), 7.28–7.37 (*m*, 1H, ArH), 4.34 (*t*, 2H, ^3J = 7.2 Hz, −N−CH_2−), 1.80–1.90 (m, 2H, −N−C−CH_2−), 1.29–1.58 (*m*, 6H, −$(CH_2)_3$−), 0.88 (t, 3H, −CH_3). IR (KBr, cm^{-1}), 3061, 2953, 2927, 2855, 2212, 1904, 1858, 1808, 1594, 1473, 1356, 1323, 1248, 1159, 1138, 1023, 908, 848, 802, 753, 727, 610. Element Anal. Calc. for $C_{19}H_{20}N_2$ (%): C, 82.57; H, 7.29; N, 10.14. Found: C, 82.41; H, 7.38; N, 10.21.

2.1.5. 3-(1H-tetrazol-5-yl)-9-hexyl-9H-carbazole **(4)**

3-Cyano-9-hexyl-9*H*-carbazole (**3**) (4.14 g, 15.0 mmol), sodium azide (14.63 g, 225.0 mmol) and ammonium chloride (12.04 g, 225.0 mmol) were added to DMF (150 mL) with mechanical agitation and the mixture was heated to 120 °C for 72 h. The cooled reaction mixture were poured into ice-water (about 1 L) and acidified with HCl to pH ≈ 1.0. The precipitants were then filtered and washed with plenty of water, dried in vacuum. Yield 84% (4.00 g), white solid, mp 225 °C (DSC). ^{1}H NMR (300 MHz, DMSO-D_6, 25 °C, ppm): δ = 8.86 (*s*, 1H, ArH), 8.24 (*d*, 1H, ^3J = 7.8 Hz, ArH),

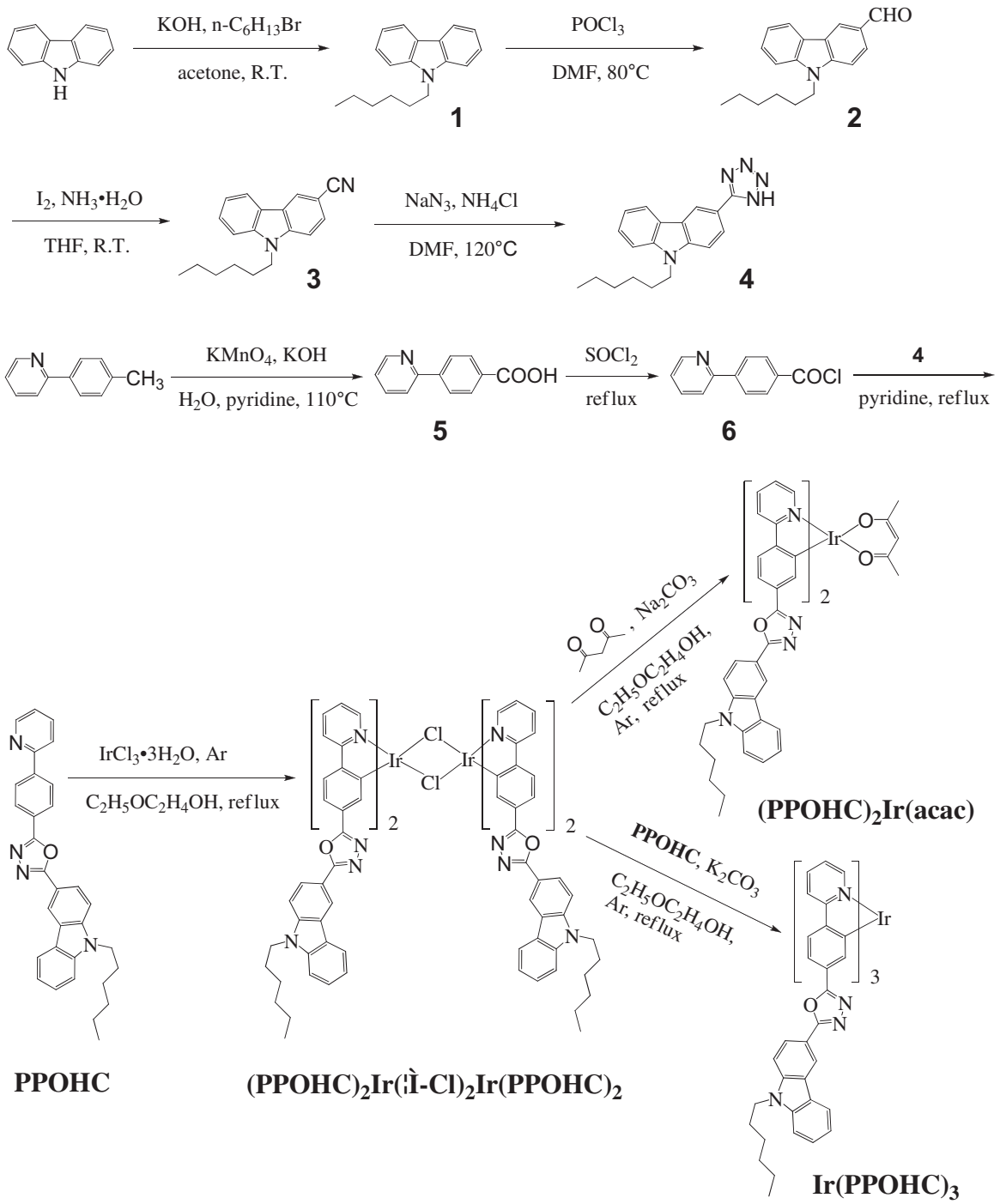

Scheme 1. Synthetic routes of iridium complexes.

8.12 (*d*, 1H, ^3J = 8.7 Hz, ArH), 7.82 (*d*, 1H, ^3J = 8.7 Hz, ArH), 7.66 (*d*, 1H, ^3J = 8.1 Hz, ArH), 7.52 (*t*, 1H, ArH), 7.28 (*t*, 1H, ArH), 4.44 (*t*, 2H, ^3J = 6.0 Hz, −N−CH_2−), 1.71–1.86 (*m*, 2H, −N−C−CH_2−), 1.17–1.35 (*m*, 6H, −$(CH_2)_3$−), 0.79 (*t*, 3H, −CH_3). IR (KBr, cm^{-1}), 3421, 3062, 2955, 2926, 2855, 2771, 2722, 2631, 1883, 1812, 1632, 1602, 1570, 1491, 1468, 1447, 1404, 1378, 1355, 1246, 1196, 1158, 1056, 996, 909, 808, 749, 723. Element Anal. Calc. For $C_{19}H_{21}N_5$ (%): C, 71.45; H, 6.63; N, 21.93. Found (%): C, 71.28; H, 6.75; N, 21.97.

*2.1.6. 4-(Pyridin-2-yl)benzoic acid **(5)***

KOH (2.80 g, 50.0 mmol) and 2-*p*-tolylpyridine (5.08 g, 30.0 mmol) were added to a mixture of water (30 mL) and pyridine (50 mL), and heated to 110 °C. A saturated aqueous solution of $KMnO_4$ (7.11 g, 45.0 mmol) was added dropwise into the aforementioned mixture with stirring. The stirring was kept until the purple of the permanganate vanished (checked by dropping the solution on the filter paper), then the hot mixture was filtered on a vacuum filter, the filter residue washed with hot water (3 × 30 mL). The filtrate was carefully adjusted to pH = 7.0 with concentrated hydrochloric acid after it was cooled to room temperature, a large quantity of white precipitate was produced and collected on a vacuum filter, washed with water and dried in vacuum. Yield 65% (3.88 g), white solid, mp 237 °C (DSC). ^{1}H NMR (300 MHz, DMSO-D_6, 25 °C, ppm): δ = 13.04 (*s*, 1H, −COOH), 8.70–8.73 (*m*, 1H, ArH), 8.70–8.73 (*m*, 2H, ArH), 8.04–8.07 (*m*, 3H,

ArH), 7.87–7.91 (*q*, 1H, ArH), 7.40–7.44 (*m*, 1H, ArH). IR (KBr, cm^{-1}), 3551, 3415, 3084, 3028, 2922, 2791, 2595, 2468, 1874, 1691, 1597, 1473, 1435, 1406, 1288, 1264, 1183, 1159, 1123, 1003, 811, 760. Element Anal. Calc. for $C_{12}H_9NO_2$ (%): C, 72.35; H, 4.55; N, 7.03. Found (%): C, 72.48; H, 4.72; N, 6.85.

2.1.7. 3-(5-(4-(Pyridin-2-yl)phenyl)-1,3,4-oxadiazol-2-yl)-9-hexyl-9H-carbazole (PPOHC)

4-(Pyridin-2-yl)benzoic acid (2.99 g, 15.0 mmol) was added into $SOCl_2$ (50 mL) and refluxed for 12 h to give 4-(pyridin-2-yl)benzoyl chloride (**6**). The excess $SOCl_2$ was removed by vacuum distillation. After 4-(pyridin-2-yl)benzoyl chloride was cooled to room temperature, the solution of 3-(1*H*-tetrazol-5-yl)-9-hexyl-9*H*-carbazole (**4**) (4.79 g, 15.0 mmol) in anhydrous pyridine (80 mL) was added dropwise in and then stirred under reflux in the presence of N_2 for 6 h. After the reaction mixture was cooled to room temperature, it was poured into the water (about 500 mL). The precipitate was collected on a vacuum filter and washed with water. The pure product was obtained by silica gel column chromatography, eluting with petroleum ether (60–90 °C) and CH_2Cl_2 (volume ratio, 1:1). Yield 73% (5.18 g), white solid, mp 165 °C (DSC). ^{1}H NMR (300 MHz, $CDCl_3$, 25 °C, ppm): δ = 8.90 (*s*, 1H, ArH), 8.77–8.79 (*q*, 1H, ArH), 8.21–8.33 (*m*, 6H, ArH), 7.83 (*t*, 2H, ArH), 7.46–7.58 (*m*, 3H, ArH), 7.28–7.36 (*m*, 2H, ArH), 4.37 (*t*, 2H, ^3J = 6.6 Hz, –N–CH_2–), 1.85–1.95 (*m*, 2H, –N–C–CH_2–), 1.28–1.44 (m, 6H, –$(CH_2)_3$–), 0.90 (*t*, 3H, –CH_3). IR (KBr, cm^{-1}), 3049, 2956, 2925, 2853, 1950, 1880, 1780, 1600, 1560, 1494, 1460, 1433, 1326, 1253, 1216, 1190, 1143, 1097, 1062, 1013, 989, 964, 892, 856, 812, 785, 752, 731. MS (ESI, m/z): 473.3 $[M + H]^+$. Element Anal. Calc. for $C_{31}H_{28}N_4O$ (%): C, 78.79; H, 5.97; N, 11.86. Found (%): C, 78.67; H, 6.08; N, 11.93.

2.1.8. $(PPOHC)_2Ir(\mu\text{-}Cl)_2Ir(PPOHC)_2$

$IrCl_3 \cdot 3H_2O$ (0.42 g, 1.2 mmol), PPOHC (1.28 g, 2.7 mmol) and H_2O (8 mL) were added in 2-methoxyethanol (24 mL). The mixture was heated under reflux and argon for 24 h and then cooled to room temperature. The yellow precipitate was collected on a filter and washed by water and methanol alternately. Yield 76% (1.21 g), yellow solid. The dimer product was directly used for the next step after being dried in vacuum without further purification and characterization.

2.1.9. $(PPOHC)_2Ir(acac)$

Chloro-bridged dimer $(PPOHC)_2Ir(\mu\text{-}Cl)_2Ir(PPOHC)_2$ (0.70 g, 0.3 mmol), acetylacetone (0.30 g, 3.0 mmol), and Na_2CO_3 (0.80 g, 7.5 mmol) in 2-ethoxyethanol (15 ml) was heated under reflux and argon for 24 h. The reaction mixture was poured in water (about 150 mL) after it was cooled to room temperature. The orange–yellow precipitate was collected on a filter and washed by water and methanol alternately. The crude product was purified by silica gel column chromatography with petroleum ether (60–90 °C)/CH_2Cl_2/$CH_3COOC_2H_5$ (volume ratio, 2:6:1) as eluent to afford pure product. Yield 23% (160 mg), orange–yellow solid. ^{1}H NMR (300 MHz, $CDCl_3$, 25 °C, ppm): δ = 8.68 (*d*, 4H, ^3J = 5.1 Hz, ArH), 8.16 (*d*, 2H, ^3J = 7.8 Hz, ArH), 8.03–8.11 (*q*, 4H, ArH), 7.94 (*t*, 2H, ^3J = 7.5 Hz, ArH), 7.79 (*d*, 2H, ^3J = 6.3 Hz, ArH), 7.72 (*d*, 2H, ^3J = 8.1 Hz, ArH), 7.64 (*d*, 2H, ^3J = 7.8 Hz, ArH), 7.27–7.56 (*m*, 10H, ArH), 5.30 (*s*, 1H, acac–CH), 4.32 (*t*, 4H, ^3J = 7.2 Hz, –N–CH_2–), 1.82–1.89 (*m*, 4H, –N–C–CH_2–), 1.57 (*s*, 6H, acac–CH_3), 1.15–1.37 (*m*, 12H, –$(CH_2)_3$–), 0.88 (*t*, 6H, –CH_3). IR (KBr, cm^{-1}), 3055, 2953, 2927, 2855, 2039, 1600, 1579, 1543, 1516, 1468, 1431, 1395, 1353, 1250, 1155, 1060, 1022, 963, 892, 810, 782, 749, 729. MS (ESI, m/z): 1234.6 $[M]^+$. Element Anal. Calc. for $C_{67}H_{61}IrN_8O_4$ (%): C, 65.19; H, 4.98; N, 9.08. Found (%): C, 65.28; H, 5.06; N, 9.18.

2.1.10. $Ir(PPOHC)_3$

Chloro-bridged dimer $(PPOHC)_2Ir(\mu\text{-}Cl)_2Ir(PPOHC)_2$ (0.35 g, 0.15 mmol), PPOHC (0.16 g, 0.34 mmol), and K_2CO_3 (0.47 g, 3.4 mmol) in 2-ethoxyethanol (15 mL) was heated under reflux and argon for 24 h. The reaction mixture was poured in water (about 150 mL) after it was cooled to room temperature. The orange–yellow precipitate was collected on a filter and washed by water and methanol alternately. The crude product was purified by silica gel column chromatography with petroleum ether (60–90 °C)/CH_2Cl_2/$CH_3COOC_2H_5$ (volume ratio, 2:6:1) as eluent to afford pure product. Yield 21% (101 mg), orange–yellow solid. ^{1}H NMR (300 MHz, $CDCl_3$, 25 °C, ppm): δ = 8.83–9.28 (*m*, 3H, ArH), 8.63–8.74 (*m*, 3H, ArH), 8.24–8.55 (*m*, 3H, ArH), 8.07–8.20 (*m*, 6H, ArH), 7.88–8.00 (*m*, 4H, ArH), 7.63–7.85 (*m*, 6H, ArH), 7.28–7.55 (*m*, 12H, ArH), 7.15–7.22 (*m*, 2H, ArH), 6.50–7.05 (*m*, 3H, ArH), 4.33 (*t*, 6H, ^3J = 6.9 Hz, –N–CH_2–), 1.87–1.91 (*m*, 6H, –N–C–CH_2–), 1.10–1.42 (*m*, 18H, –$(CH_2)_3$–), 0.88 (*t*, 9H, –CH_3). IR (KBr, cm^{-1}), 3053, 2952, 2926, 2855, 2037, 2016, 1600, 1562, 1541, 1487, 1466, 1430, 1385, 1352, 1325, 1249, 1153, 1059, 1024, 963, 893, 809, 781, 748, 728. MS (ESI, m/z): 1607.8 $[M + H]^+$. Element Anal. Calc. for $C_{93}H_{81}IrN_{12}O_3$ (%): C, 69.51; H, 5.08; N, 10.46. Found (%): C, 69.38; H, 5.17; N, 10.62.

2.2. Fabrication and measurements of EL devices

Indium-tin oxide (ITO) coated glass with a sheet resistance of 15–20 Ω/□ was used as substrate anode and was cleaned with detergents, then with deionized water, acetone and isopropanol in an ultrasonic bath. After oxygen plasma cleaning for 4 min, an anode buffer layer of poly(3,4-ethylenedioxythiophene) doped with poly(styrene sulfonate) (PEDOT:PSS) was spin-coated on the ITO substrate and then dried by baking in a vacuum oven at 80 °C for 8 h. Then a light-emitting layer consisted of host materials poly(N-vinylcarbazole) (PVK), electron-transporting materials 2-(4-biphenylyl)-5-4-*tert*-butylphenyl-1,3,4-oxadiazole (PBD, used in yellow-light devices) or 1,3-bis[(4-*tert*-butylphenyl)-1,3,4-oxadiazolyl]phenylene (OXD-7, used in white-light devices), and dopants of iridium(III) complexes $(PPOHC)_2Ir(acac)$ or $Ir(PPOHC)_3$ at different concentrations was spin-coated on the PEDOT: PSS layer in a glove box (Vacuum Atmosphere Co.) containing less than 10 ppm oxygen and moisture, then was baked on a hot plate at 100 °C in inert atmosphere for 20 min to remove solvent (chlorobenzene) residue. Electron-transporting layer, electron injection layer (CsF) and subsequent cathode layer (Al) were thermally evaporated with a base pressure of 3×10^{-4} Pa. The spin-coated film thickness was measured by an Alfa Step 500 surface profilometer (Tencor), layer thickness during thermal deposition was monitored by a quartz crystal thickness/ratio monitor (Model: STM-100/MF, Sycon). The current density–luminance–voltage (I–L–V) characteristics were measured using a Keithley 236 source measurement unit and a calibrated silicon photodiode. EL spectra

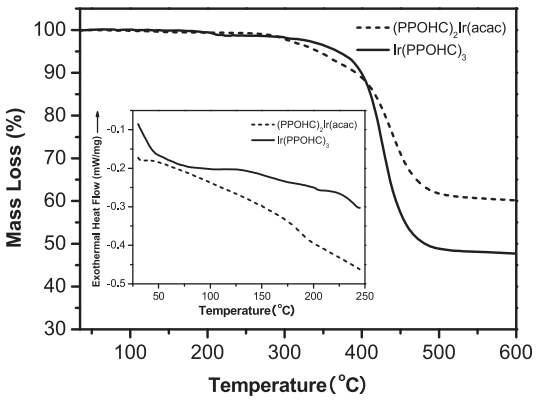

Fig. 1. TG and DSC (inset) curves of the complexes.

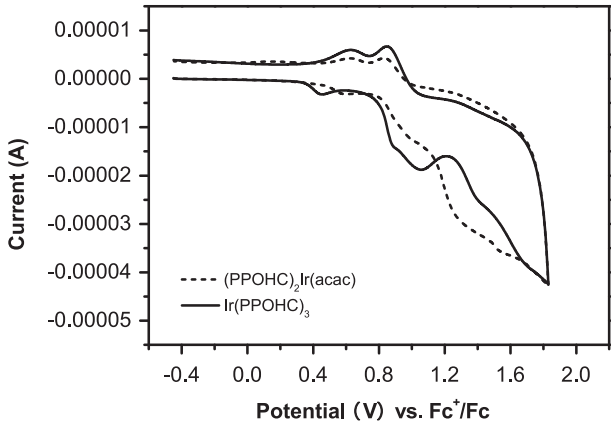

Fig. 2. CV curves of the complexes in CH_2Cl_2 solution of 1×10^{-3} mol/L. Potentials were recorded versus Fc^+/Fc (Fc is ferrocene).

and the Commission Internationale de L'Eclairage (CIE) coordinate were recorded using a spectrophotometer (SpectraScan PR-705, Photo Research).

3. Results and discussion

3.1. Synthesis

The synthesis procedure employed to obtained the iridium complexes is shown in Scheme 1. The ligand PPOHC was synthesized via a similar procedure to the reported by Lee [37], but 3-formyl-9-hexyl-9H-carbazole (**2**) was reduced to 3-cyano-9-hexyl-9H-carbazole (**3**) by using I_2 instead of NH_2OH as reductant at room temperature in 1.5 h, which constitutes a simpler and milder reduction reaction. The iridium complexes were synthesized from PPOHC and $IrCl_3 \cdot 3H_2O$ by a conventional way via iridium dimer [14–17].

3.2. Thermal properties

Thermogravimetry (TG) and differential scanning calorimetry (DSC) curves of the iridium complexes are shown in Fig. 1. Complexes $(PPOHC)_2Ir(acac)$ and $Ir(PPOHC)_3$ have high thermal stability with 5% weight-reduction temperatures ($\Delta T_{5\%}$) of 343 °C and 370 °C, respectively. DSC curves show there is neither crystallization nor melting peaks. The glass-transition temperatures (T_g) of $(PPOHC)_2Ir(acac)$ and $Ir(PPOHC)_3$ are 188 °C and 201 °C, respectively. The amorphous character and high T_g of the iridium complexes are resistant to crystallization and phase disengagement, and are desirable for EL devices with high stability and efficiency [38,39]. The results suggest that the n-hexyl substituent on the carbazole unit plays a significant role in improving the amorphous nature and T_g values as well as the solubility [39,40].

Table 1
Electrochemical properties.

Complex	$E_{1/2,ox}$ (V)[a]	$E_{onset,ox}$ (V)[a]	HOMO (eV)	LUMO (eV)[b]	E_g (eV)
$(PPOHC)_2Ir(acac)$	0.61	0.48	−5.28	−2.92	2.36
$Ir(PPOHC)_3$	0.54	0.36	−5.16	−2.73	2.43

[a] Measured in Ar–saturated CH_2Cl_2, 0.1 mol/L $TBAPF_6$, scan rate 50 mV/s, vs. Fc^+/Fc couple.
[b] LUMO = HOMO + E_g.

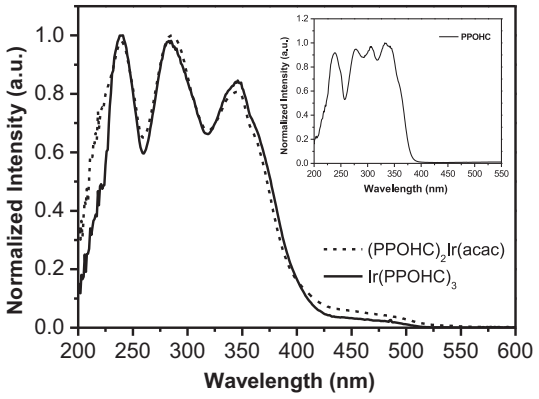

Fig. 3. UV–Vis absorption spectra of the complexes and ligand (inset) in CH_2Cl_2 solution of 2.0×10^{-5} M.

3.3. Electrochemical properties

The cyclic voltammetry (CV) curves of the complexes are shown in Fig. 2. All the complexes exhibit a one-electron reversible oxidation couple at relatively low positive potentials and an irreversible oxidation couple at relatively high positive potentials. The former are attributed to a metal-centered Ir^{III}/Ir^{IV} oxidation couple [14,40], the latter may originate from the electron-donating carbazole unit [40,41]. The oxidation potential of homoleptic complex $Ir(PPOHC)_3$ is lower than that of heteroleptic complex $(PPOHC)_2Ir(acac)$ and these values are similar to those of other homoleptic and heteroleptic iridium complex homologs in the literature [14]. The value of the energy gap (E_g) of every iridium(III) complex was obtained from the spectroscopy absorption edge ($E_g = 1240/\lambda_{a,edge}$) [14,42], together with the oxidation potentials, the HOMO and LUMO energy levels relative to the energy level of ferrocene (4.8 eV under vacuum) can be estimated [14], the results are listed in Table 1.

3.4. UV–Vis absorption and PL properties

The UV–Vis absorption spectra of the complexes in solution are shown in Fig. 3. The absorption spectra of the complexes $(PPOHC)_2Ir(acac)$ and $Ir(PPOHC)_3$ strongly resemble each other, that indicates the absorption spectra are mainly decided by the PPOHC ligand and the ancillary ligand, acetylacetone, scarcely plays a role in the absorption in $(PPOHC)_2Ir(acac)$ [38]. The strong absorption bands at 200–420 nm can be assigned to the spin-allowed $^1\pi$–π^*

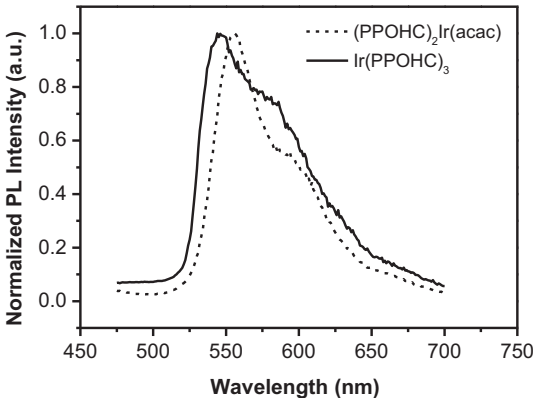

Fig. 4. PL spectra of the complexes in CH_2Cl_2 solution of 2.0×10^{-5} M.

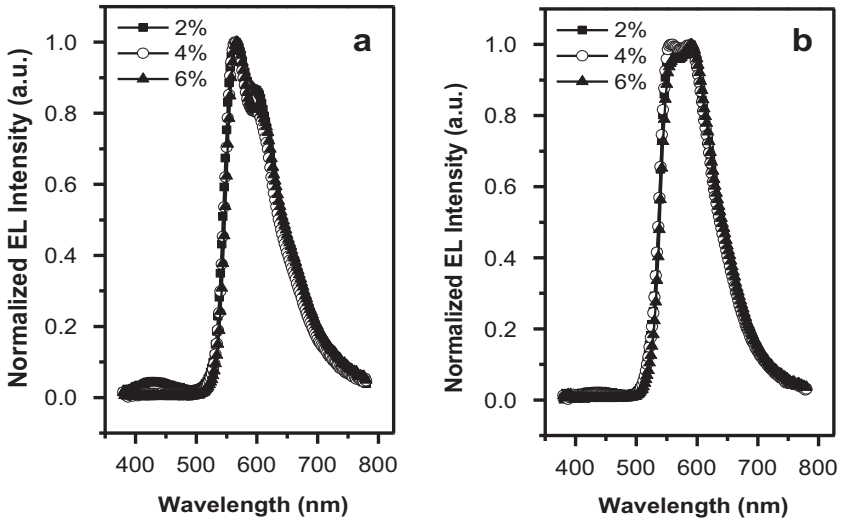

Fig. 5. EL spectra of the complexes $(PPOHC)_2Ir(acac)$ (a) and $Ir(PPOHC)_3$ (b). Device configuration: ITO/PEDOT: PSS/PVK: PBD: complex (70: 30: x)/TPBI/CsF/Al.

transition of the ligand PPOHC in the complexes. In contrast to the absorption spectrum of PPOHC in CH_2Cl_2 solution, such strong absorption bands have a small red shift and slight differentiation due to the conjugated coordination. The weak absorption bands (at 420–525 nm for $(PPOHC)_2Ir(acac)$ and 420–510 nm for $Ir(PPOHC)_3$) can be assigned to an admixture of ^{1}MLCT (metal–ligand charge transfer), ^{3}MLCT and $^3\pi-\pi^*$ states [33,38]. The admixture of ^{3}MLCT and $^3\pi-\pi^*$ with higher-lying ^{1}MLCT is due to the strong spin–orbit coupling induced by the iridium heavy atom [9,33,38].

The PL spectra of $(PPOHC)_2Ir(acac)$ and $Ir(PPOHC)_3$ in solution (λ_{ex} = 350 nm) are shown in Fig. 4. The PL spectra of complexes $(PPOHC)_2Ir(acac)$ and $Ir(PPOHC)_3$ also resemble each other, both of them have a maximum main peak and a shoulder peak, but the PL spectra of complex $(PPOHC)_2Ir(acac)$ (λ_{max} = 555 nm) gives a red shift of 9 nm in comparison with that of $Ir(PPOHC)_3$ (λ_{max} = 546 nm) due to higher ligand-field strength of acetylacetonate anion than PPOHC anion [14].

3.5. Device performances

Polymeric light-emitting diodes were fabricated with the configurations of ITO/PEDOT:PSS (40 nm)/emitting layer (70 nm)/TPBI (30 nm)/CsF (1.5 nm)/Al (120 nm), emitting layer: PVK (70 wt.-%) : PBD (30 wt.-%) : complex (*x* wt.-%). The emitting layers consisted of host materials PVK, electron-transporting materials PBD, and dopants of the complexes $(PPOHC)_2Ir(acac)$ or $Ir(PPOHC)_3$ at different concentrations (2, 4, 6 wt.-%); 1,3,5-tris(N-phenylbenzimidazol-2-yl)-benzene (TPBI) was used as hole-blocking/electron-transporting material.

Table 2
Device performance of the complexes[a].

Dopant	concentration (wt.-%)	V_{on} (V)	L_{max} (cd/m^2)	LE_{max} (cd/A)	QE_{max} (%)	λ_{max} (nm)	CIE[b]
$(PPOHC)_2Ir(acac)$	2	7.0	3793	7.6	3.0	564	(0.51, 0.46)
	4	7.0	6354	11.1	4.4	564	(0.52, 0.47)
	6	7.5	4020	7.6	3.1	566	(0.52, 0.47)
$Ir(PPOHC)_3$	2	5.6	4079	10.3	4.1	588	(0.50, 0.47)
	4	6.0	6323	16.4	6.6	560	(0.50, 0.49)
	6	6.3	6178	15.8	6.3	590	(0.51, 0.48)

[a] Device configuration: ITO/PEDOT: PSS/PVK: PBD: complex/TPBI/CsF/Al.
[b] at 12 mA/m^2.

EL spectra of devices are shown in Fig. 5. The weak emission in the region of 400–480 nm originated from the PVK–PBD exciplex [43] can be observed when the doping concentrations of the complexes are 2 wt.-%, however, such emission peaks have not emerged at 4 wt.-% and 6 wt.-%, because the low doping concentrations are not enough to consume the excitons of the PVK. Relative to the PL spectra of the complexes in solution, the EL spectra show red shifts of 9–15 nm due to closer intermolecular contacts in the solid-state [44]. The EL spectrum of $(PPOHC)_2Ir(acac)$ resembles closely its PL spectrum, however, the EL spectrum of $Ir(PPOHC)_3$ resembles its PL spectrum less so, the low shoulder on the peak on the right side of the PL spectrum has become more intense in the EL spectrum, and this disparity was possibly caused by slight optical microcavity effect [45,46].

The device performances are listed in the Table 2. The turn-on voltages (V_{on}) of the devices are 5.6–7.0 V, the relatively high driving voltages may be due to the large hole barrier at the PEDOT:PSS/PVK interface (HOMOs of PVK ~ 5.80 eV versus PEDOT ~ 5.20 eV) and the thicker emissive layer (70 nm) [14]. In contrast to the devices fabricated by $(PPOHC)_2Ir(acac)$, the devices fabricated by $Ir(PPOHC)_3$ have lower turn-on voltages at the same doping concentration which may be due to a closer match of the

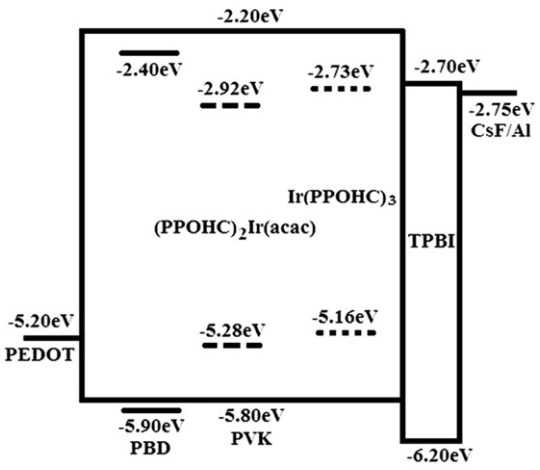

Fig. 6. Energy diagram of the materials used in the devices. Device configuration: ITO/PEDOT: PSS/PVK:PBD:complex (70:30:x)/TPBI/CsF/Al.

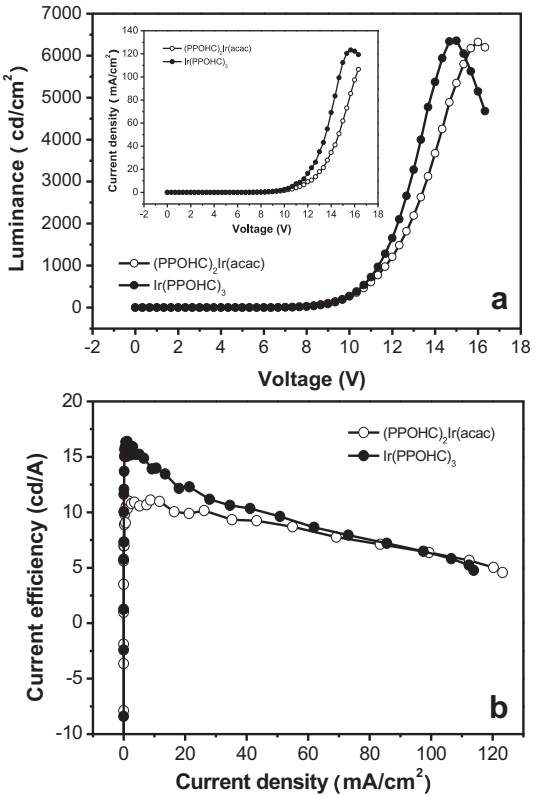

Fig. 7. Luminance and current density (inset) vs. voltage (a), and current efficiency vs. current density (b) characteristics of the devices at 4 wt.-% doping concentrations. Device configuration: ITO/PEDOT: PSS/PVK: PBD: complex (70: 30: 4)/TPBI/CsF/Al.

HOMO level of Ir(PPOHC)$_3$ with PEDOT (~5.20 eV), and the LUMO level of Ir(PPOHC)$_3$ with TPBI (~2.70 eV) (as shown in Fig. 6), which are beneficial to hole and electron injection. By comparing the performance of different dopant concentrations, it is clearly seen that 4 wt.-% is an optimal doping concentration because of the maximum efficiencies and luminances being obtained, the maximum efficiencies of the devices using (PPOHC)$_2$Ir(acac) and Ir(PPOHC)$_3$ are 11.1 cd/A and 16.4 cd/A, and the maximum luminances are 6354 cd/m^2 and 6323 cd/m^2, with CIE coordinates of (0.52, 0.47) and (0.50, 0.49) respectively.

The luminance and current density vs. voltage, and current efficiency vs. current density characteristics of the devices at 4 wt.-% doping concentrations are shown in Fig. 7. Compared with

Table 3
Device performances of the FIrpic and Ir(PPOHC)$_3$[a].

Firpic:Ir(PPOHC)$_3$ (mass ratio)	V_{on} (V)	L_{max} (cd/m^2)	LE_{max} (cd/A)	QE_{max} (%)	CIE[b] (x, y)
5:1	4.2	7873	13.7	5.3	0.41, 0.48
7.5:1	4.4	5954	12.2	4.71	0.37, 0.46
8.5:1	4.5	6275	15.3	5.5	0.39, 0.44
10:1	4.3	5047	10.5	3.4	0.29, 0.44

[a] Device configuration: ITO/PEDOT: PSS/PVK: OXD-7: FIrpic: Ir(PPOHC)$_3$/CsF/Al.
[b] at 12 mA/m^2.

(PPOHC)$_2$Ir(acac), higher luminance and current density can be observed at the same voltage for Ir(PPOHC)$_3$ due to more efficient and balanced charge injection. It can be understood from the energy level diagrams in Fig. 6 that the closer match of the HOMO level of Ir(PPOHC)$_3$ with PEDOT and the LUMO level of Ir(PPOHC)$_3$ with TPBI can decrease the hole and electron migrating barrier. The current efficiency of Ir(PPOHC)$_3$ declines relatively faster with the increase of current density at low current density (<20 mA/cm^2), this may be attributed to the faster increase of triplet–triplet (T–T) annihilation and field-induced quenching effects [14], however, both Ir(PPOHC)$_3$ and (PPOHC)$_2$Ir(acac) declines slowly with the increase of current density at high current efficiency. The current efficiency of Ir(PPOHC)$_3$ is higher than that of (PPOHC)$_2$Ir(acac) even at a high current density near 100 mA/cm^2, so Ir(PPOHC)$_3$ is a better electroluminescent phosphor for OLEDs.

The white polymeric light-emitting diodes were fabricated by doping of Ir(PPOHC)$_3$ and blue light-emitting FIrpic in PVK matrix. The configuration of the devices are ITO/PEDOT: PSS (40 nm)/emitting layer (80 nm)/CsF (1.5 nm)/Al (120 nm), emitting layer is PVK (63 wt.-%): OXD-7 (27 wt.-%): dopants (FIrpic and Ir(PPOHC)$_3$, 10 wt.-%). OXD-7 was electron-transporting material. The FIrpic and Ir(PPOHC)$_3$ were doped at different mass ratios of 5:1, 7.5:1, 8.5:1 and 10:1.

The EL spectra are shown in Fig. 8 and the performances are list in Table 3. The emission in the region of 450–530 nm and 530–700 nm originate from FIrpic and Ir(PPOHC)$_3$, respectively [47]. The relative EL intensity of FIrpic increases with the increase of its doping concentration, at the same time, the intensity of Ir(PPOHC)$_3$ decreases. When the mass ratio of FIrpic:Ir(PPOHC)$_3$ is 8.5:1, both emission of FIrpic and Ir(PPOHC)$_3$ are sufficient in magnitude and balanced, so this mass ratio is an optimal ratio for obtaining white-light. The turn-on voltage of the device at this mass ratio is 4.5 V, the maximum luminance and efficiency are 6275 cd/m^2 (at 13 V) and 15.3 cd/A respectively, with the CIE coordinates of (0.39, 0.44). The luminance, current density vs. voltage and current efficiency vs. current density characteristics of

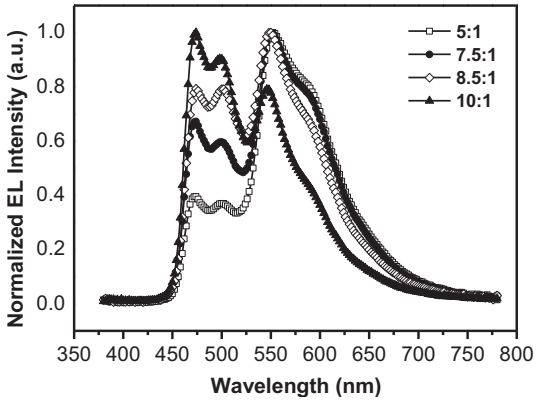

Fig. 8. EL spectra of the white-light devices based on the FIrpic and Ir(PPOHC)$_3$. Device configuration: ITO/PEDOT: PSS/PVK: OXD-7: FIrpic: Ir(PPOHC)$_3$/CsF/Al.

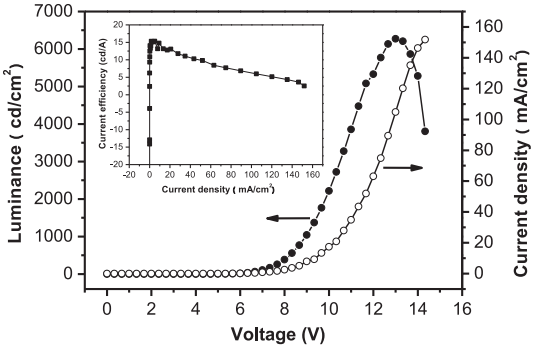

Fig. 9. Luminance and current density vs. voltage, and efficiency vs. current density (inset) characteristics of the white-light device. Device configuration: ITO/PEDOT: PSS/PVK: OXD-7: FIrpic: Ir(PPOHC)$_3$ (8.5: 1)/CsF/Al.

the device at this optimal mass ratio are shown in Fig. 9. The current efficiency declines slowly with increasing current density nearly linear, the current efficiency remains 10 cd/A at near 50 mA/cm^2, and still remains 6 cd/A at high current density near 100 mA/cm^2. By comparison with the EL efficiencies declining quickly with increasing current density in a decurved line of some OLEDs [42,48], the results indicate that the device possesses good stability.

4. Conclusions

The ligand 3-(5-(4-(pyridin-2-yl)phenyl)-1,3,4-oxadiazol-2-yl)-9-hexyl-9*H*-carbazole (PPOHC) and its iridium(III) complexes $(PPOHC)_2Ir(acac)$ and $Ir(PPOHC)_3$ were synthesized. The $(PPOHC)_2Ir(acac)$ and $Ir(PPOHC)_3$ complexes have high thermal stability with 5% weight-reduction temperatures ($\Delta T_{5\%}$) of 343 °C and 370 °C, and glass-transition temperatures (T_g) of 188 °C and 201 °C, respectively. The polymeric light-emitting diodes using $(PPOHC)_2Ir(acac)$ or $Ir(PPOHC)_3$ as the dopant emitters showed maximum efficiencies of 11.1 cd/A and 16.4 cd/A respectively. The mass ratio of FIrpic:$Ir(PPOHC)_3$ (8.5:1) was an optimal ratio for the white-light device, and a maximum efficiency of 15.3 cd/A was obtained with CIE coordinates of (0.39, 0.44).

Acknowledgments

This work was supported by China Postdoctoral Science Foundation (No. 20090450858), the National Natural Science Foundation of China (Nos.U0634003 and 21074038), and State Key Basical Research Project of China (Nos. 2009CB623602 and 2009CB930604).

References

[1] Tang CW, VanSlyke SA. Organic electroluminescent diodes. Appl Phys Lett 1987;51:913–5.
[2] Burroughes JH, Bradley DDC, Brown AR, Marks RN, Mackay K, Friend RH, et al. Light-emitting diodes based on conjugated polymers. Nature 1990;347:539–41.
[3] D'Andrade BW, Forrest SR. White organic light-emitting devices for solid-state lighting. Adv Mater 2004;16:1585–95.
[4] Holder E, Langeveld BMW, Schubert US. New trends in the use of transition metal–ligand complexes for applications in electroluminescent devices. Adv Mater 2005;17:1109–21.
[5] Misra A, Kumar P, Kamalasanan MN, Chandra S. White organic LEDs and their recent advancements. Semicond Sci Technol 2006;21:R35–47.
[6] Grimsdale AC, Chan KL, Martin RE, Jokisz PG, Holmes AB. Synthesis of light-emitting conjugated polymers for applications in electroluminescent devices. Chem Rev 2009;109:897–1091.
[7] Wong W-Y, Ho C-L. Heavy metal organometallic electrophosphors derived from multi-component chromophores. Coord Chem Rev 2009;253:1709–58.
[8] Baldo MA, O'Brien DF, You Y, Shoustikov A, Sibley S, Thompson ME, et al. Highly efficient phosphorescent emission from organic electroluminescent devices. Nature 1998;395:151–4.
[9] Lamansky S, Djurovich P, Murphy D, Abdel-Razzaq F, Lee H-E, Adachi C, et al. Highly phosphorescent bis-cyclometalated iridium complexes: synthesis, photophysical characterization, and use in organic light emitting diodes. J Am Chem Soc 2001;123:4304–12.
[10] Evans RC, Douglas P, Winscom CJ. Coordination complexes exhibiting room-temperature phosphorescence: evaluation of their suitability as triplet emitters in organic light emitting diodes. Coord Chem Rev 2006;250:2093–126.
[11] Zeng W, Wu H, Zhang C, Huang F, Peng J, Yang W, et al. Polymer light-emitting diodes with cathodes printed from conducting Ag paste. Adv Mater 2007;19:810–4.
[12] Jiang J, Xu Y, Yang W, Guan R, Liu Z, Zhen H, et al. High-efficiency white-light-emitting devices from a single polymer by mixing singlet and triplet emission. Adv Mater 2006;18:1769–73.
[13] Wu H, Zhou G-J, Zou J, Ho C-L, Wong W-Y, Yang W, et al. Efficient polymer white-light-emitting devices for solid-state lighting. Adv Mater 2009;21:1–4.
[14] Ho C-L, Wong W-Y, Zhou G-J, Yao B, Xie Z, Wang L. Solution-processible multi-component cyclometalated iridium phosphors for high-efficiency orange-emitting OLEDs and their potential use as white light sources. Adv Funct Mater 2007;17:2925–36.
[15] Zhang X, Chen Z, Yang C, Li Z, Zhang K, Yao H, et al. Highly efficient polymer light-emitting diodes using color-tunable carbazole-based iridium complexes. Chem Phys Lett 2006;22:386–90.
[16] Tian N, Thiessen A, Schiewek R, Schmitz OJ, Hertel D, Meerholz K, et al. Efficient synthesis of carbazolyl- and thienyl-substituted β-diketonates and properties of their red- and green-light-emitting Ir(III) complexes. J Org Chem 2009;74:2718–25.
[17] Wu H, Zou J, Liu F, Wang L, Mikhailovsky A, Bazan GC, et al. Efficient single active layer electrophosphorescent white polymer light-emitting diodes. Adv Mater 2008;20:696–702.
[18] Huang F, Shih P-I, Shu C-F, Chi Y, Jen Alex K-Y. Highly efficient polymer white-light-emitting diodes based on lithium salts doped electron transporting layer. Adv Mater 2009;21:361–5.
[19] Tsujimoto H, Yagi S, Asuka H, Inui Y, Ikawa S, Maeda T, et al. Pure red electrophosphorescence from polymer light-emitting diodes doped with highly emissive bis-cyclometalated iridium(III) complexes. J Organomet Chem 2010;695:1972–8.
[20] You YM, Park SY. Phosphorescent iridium(III) complexes: toward high phosphorescence quantum efficiency through ligand control. Dalton Trans; 2009:1267–82.
[21] Zhao Q, Liu S-J, Huang W. Promising optoelectronic materials: polymers containing phosphorescent iridium(III) complexes. Macromol Rapid Commun 2010;31:794–807.
[22] Cheng Y-J, Liu M, Zhang Y, Niu Y, Huang F, Ka J-W, et al. Thermally cross-linkable hole-transporting materials on conducting polymer: synthesis, characterization, and applications for polymer light-emitting devices. Chem Mater 2008;20:413–22.
[23] Cheng F, Bian Z, Huang C. Progresses in electroluminescence based on europium(III) complexes. J Rare Earths 2009;27:345–55.
[24] Tao Y, Wang Q, Yang C, Wang Q, Zhang Z, Zou T, et al. A simple carbazole/oxadiazole hybrid molecule: an excellent bipolar host for green and red phosphorescent OLEDs. Angew Chem 2008;120:8224–7.
[25] Tao Y, Wang Q, Shang Y, Yang C, Ao L, Qin J, et al. Multifunctional bipolar triphenylamine/oxadiazole derivatives: highly efficient blue fluorescence, red phosphorescence host and two-color based white OLEDs. Chem Commun; 2009:77–9.
[26] Tao Y, Wang Q, Yang C, Zhong C, Zhang K, Qin J, et al. Tuning the optoelectronic properties of carbazole/oxadiazole hybrids through linkage modes: hosts for highly efficient green electrophosphorescence. Adv Funct Mater 2010;20:304–11.
[27] He Z, Wong W-Y, Yu XM, Kwok H-S, Lin ZY. Phosphorescent platinum(II) complexes derived from multifunctional chromophores: synthesis, structures, photophysics, and electroluminescence. Inorg Chem 2006;45:10922–37.
[28] Chiang CC, Chen H-C, Lee C-S, Leung M-K, Lin K-R, Hsieh K-H. Electrochemical deposition of bis(N, N′-diphenylaminoaryl) substituted ferrocenes, and their application as a hole-injection layer on polymeric light-emitting diodes. Chem Mater 2008;20:540–52.
[29] Tang H, Tang H, Zhang Z, Yuan J, Cong C, Zhang K. Synthesis, photoluminescent and electroluminescent properties of a novel europium(III) complex involving both hole- and electron-transporting functional groups. Synth Met 2009;159:72–7.
[30] Huang W-S, Lin J, Chien C-H, Tao Y-T, Sun S-S, Wen Y-S. Highly phosphorescent bis-cyclometalated iridium complexes containing benzoimidazole-based ligands. Chem Mater 2004;16:2480–8.
[31] Wang Q, Ding J, Ma D, Cheng Y, Wang L, Jing X, et al. Harvesting excitons via two parallel channels for efficient white organic LEDs with nearly 100% internal quantum efficiency: fabrication and emission-mechanism analysis. Adv Funct Mater 2009;19:84–95.
[32] Wang Q, Ding J, Ma D, Cheng Y, Wang L. Highly efficient single-emitting-layer white organic light-emitting diodes with reduced efficiency roll-off. Appl Phys Lett 2009;94:103503–5.
[33] Yu X-M, Kwok H-S, Wong W-Y, Zhou G-J. High-efficiency white organic light-emitting devices based on a highly amorphous iridium(III) orange phosphor. Chem Mater 2006;18:5097–103.
[34] Yu X-M, Zhou G-J, Lam C-S, Wong W-Y, Zhu X-L, Sun J-X, et al. A yellow-emitting iridium complex for use in phosphorescent multiple-emissive-layer white organic light-emitting diodes with high color quality and efficiency. J Organomet Chem 2008;693:1518–27.
[35] Liang B, Xu Y, Chen Z, Peng J, Cao Y. White polymer phosphorescent light-emitting devices with a new yellow-emitting iridium complex doped into polyfluorene. Synth Met 2009;159:1876–9.
[36] Yang L, Zhao X-H, Li Z-Y, Deng C-H, Shao G-Q, Wu J-Y, et al. Synthesis, characterization, spectroscopy and theoretical calculation of two novel carbazole derivatives. Guangpuxue Yu Guangpu Fenxi 2008;28:883–6 (in Chinese).
[37] Lee TH, Tong KL, So SK, Leung LM. Synthesis and electroluminescence of thiophene-based bipolar small-molecules with different arylamine moieties. Synth Met 2005;155:116–24.
[38] Wong W-Y, Zhou G-J, Yu X-M, Kwok H-S, Tang B-Z. Amorphous diphenylaminofluorene-functionalized iridium complexes for high-efficiency electrophosphorescent light-emitting diodes. Adv Funct Mater 2006;16:838–46.
[39] Ostrowski JC, Robinson MR, Heeger AJ, Bazan GC. Amorphous iridium complexes for electrophosphorescent light emitting devices. Chem Commun; 2002:784–5.
[40] Bettington S, Tavasli M, Bryce MR, Beeby A, Al-Attar H, Monkman AP. Tris-cyclometalated iridium(III) complexes of carbazole(fluorenyl)pyridine ligands: synthesis, redox and photophysical properties, and electrophosphorescent light-emitting diodes. Chem Eur J 2007;13:1423–31.
[41] Thomas KRJ, Velusamy M, Lin JT, Chien C-H, Tao Y-T, Wen YS, et al. Efficient red-emitting cyclometalated iridium(III) complexes containing lepidine-based ligands. Inorg Chem 2005;44:5677–85.

[42] Zhang W, Wang Y, He Z, Mu L, Zou Y, Liang C, et al. Efficient electrophosphorescence based on 2-(9,9-diethylfluoren-2-yl)-5-trifluoromethylpyridine iridium complexes. Synth Met 2010;160:354–60.
[43] Jiang X-Z, Register RA, Killeen KA, Thompson ME, Pschenitzka F, Hebner TR, et al. Effect of carbazole–oxadiazole excited-state complexes on the efficiency of dye-doped light-emitting diodes. J Appl Phys 2002;91:6717–24.
[44] Lamansky S, Djurovich P, Murphy D, Abdel-Razzaq F, Kwong R, Tsyba I, et al. Synthesis and characterization of phosphorescent cyclometalated iridium complexes. Inorg Chem 2001;40:1704–11.
[45] Vahala KJ. Optical microcavities. Nature 2003;424:839–46.
[46] Freitag P, Reineke S, Olthof S, Furno M, Lüssem B, Leo K. White top-emitting organic light-emitting diodes with forward directed emission and high color quality. Org Electron 2010;11:1676–82.
[47] Adachi C, Kwong RC, Djurovich P, Adamovich V, Baldo MA, Thompson ME, et al. Endothermic energy transfer: a mechanism for generating very efficient high-energy phosphorescent emission in organic materials. Appl Phys Lett 2001;79:2082–4.
[48] Ha Y, Seo J-H, Kim YK. Toward the saturated red phosphorescence for OLED: new iridium complexes of 2,3-bis(4-fluorophenyl)quinoxaline derivatives. Synth Met 2008;158:548–52.